TERRASAR-X INTERFEROMETRIC OBSERVATIONS OF THE RECOVERY GLACIER SYSTEM, ANTARCTICA

Dana Floricioiu[1], Nestor Yague-Martinez[1], Kenneth Jezek[2], Michael Eineder[1] and Katy Farness[2]

[1]German Aerospace Center (DLR) IMF, Oberpfaffenhofen, Germany, E-mail:dana.floricioiu@dlr.de
[2]Byrd Polar Research Center, Columbus, OH

ABSTRACT

Two methods for derivation of surface ice velocity from SAR data are presented. They are applied to the RAMP Glacier in East Antarctica, which was imaged in repeat pass by TerraSAR-X in 2008 as part of the International Polar Year (IPY). Coregistration methods and an algorithm to improve the interferometric phase quality are described. The accuracy of speckle tracking and interferometric phaseestimates of displacement are compared.

1. INTRODUCTION

The knowledge of ice flow and its variations is of great importance for glacier and ice sheet mass balance. The reaction of ice sheets to climate changes and their impact on sea level can not be understand and predicted without knowledge of ice dynamics and the amount of ice discharge to the ocean.

So far the Antarctic Ice Sheet velocity field has been derived mainly from Radarsat-1 data acquired during the Radarsat-1 Antarctic Mapping Project (RAMP) in 1997 and 2000. By rotating the satellite to collect data left of the orbital track, Radarsat-1 was the first SAR sensor capable of imaging areas south of about 80°S latitude and to the pole. Although RAMP offered the first high resolution mapping of the entire continent the interferometric coverage below 80°S was limited due to mission constraints.

Eleven years later as part of the International Polar Year (IPY) 2007-2008 the TerraSAR-X satellite initiated high resolution acquisitions in left looking mode over specific sites close to the South Pole [1]. One of these sites is the Recovery glacier system (81°S, 20°W) (Figure 1) which is of high scientific interest due to its role in discharging East Antarctic Ice to the sea. Recovery was completely imaged for the first time in 1997 during RAMP when an enigmatic tributary, now called the RAMP glacier, was discovered. While in 1997 only the northerly portion of Recovery and the confluence with its tributaries were mapped interferometrically, with TerraSAR-X three coverages of the entire RAMP glacier have been acquired enabling the derivation of the complete velocity map of the area.

In this paper, particular attention is given to the region near the onset of the RAMP ice stream (marked as red box in Figure 1). Here the fast glacier flow may be controlled by the presence of subglacial lakes and the accurate derivation of velocity is needed to understand the dynamical interplay between basal processes and flow resistance along the glacier margin.

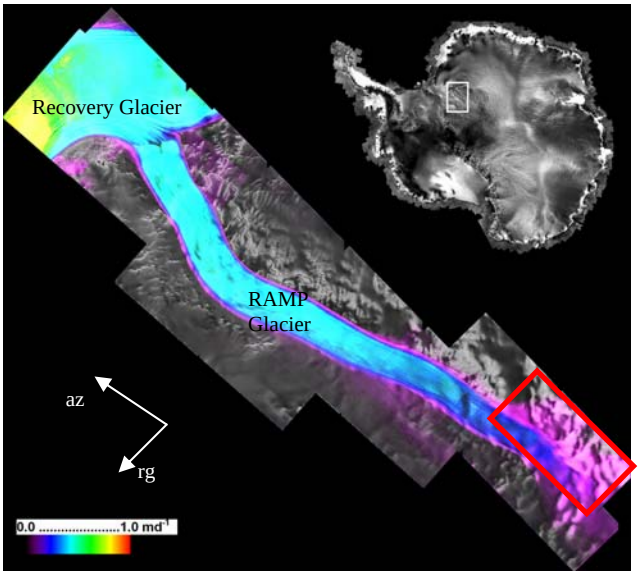

Figure 1. Mosaic of speckle tracking based surface velocities along the entire 250 km length of the RAMP tributary up to the junction with the main trunk of Recovery Glacier derived from detected TerraSAR-X products. The location is shown in the insert upper right. The red box marks the 30 x 50 km² TerraSAR-X scene at the source of the ice stream which has been InSAR processed for this paper.

2. THE TERRASAR-X OBSERVATIONS AND PREVIOUS WORK

2.1 The TerraSAR-X data set

Proc. 'Fringe 2009 Workshop', Frascati, Italy,
30 November – 4 December 2009 (ESA SP-677, March 2010)

Our investigations are based on TerraSAR-X data acquired in stripmap mode between October 2008 and January 2009. Three complete repeat pass coverages in 11-days cycles are available over the entire 250 km length of the RAMP tributary. At 45° incidence angle the slant range and azimuth resolution of the single look complex (SSC) product are about 3 m.

One particular TerraSAR-X scene at the RAMP glacier source has been InSAR processed. The area of interest was covered by a nominal stripmap scene, which has about 30 km in range x 50 km in azimuth (red box in Figure 1).

2.2 Speckle tracking results on detected products

The 11-day repeat pass TerraSAR-X data are highly coherent because no melting is present at these latitudes where snow drift or snow fall is minimal. The good coherence allowed using the amplitude correlation technique to make a mosaic of the surface velocity maps along the RAMP ice stream (Figure 1). Speckle tracking was applied to high resolution geocoded TerraSAR-X products (EEC SE) with 1.25m pixel spacing. The two components of the velocity vector were obtained with an accuracy of several cm/day. Details on the processing methodology are given in [2]. Despite its advantages the speckle tracking is not accurate for parts of the RAMP glacier where the movement is slow, e.g. at the onset of fast ice flow. Here a more accurate velocity can be obtained with InSAR as will be described in the following section.

3. METHODOLOGY

3.1 Image coregistration and interferogram generation

The fine coregistration algorithm is based on incoherent cross correlation because it is the optimum estimation of differential shift in SAR images [4]. Since the movement at the glacier source is complex and because of the high resolution of the TerraSAR-X system, coregistration polynomials are not able to follow correctly the displacement pattern. Therefore the resampling matrices were generated directly by using the image shift estimates.

In areas with high snow accumulation the backscattering coefficient is low (Figure 2a), SNR and hence coherence are low, and cross correlation delivers unstable results. Figure 2b shows the post-registration interferometric phase if coherence outliers are not removed. If the incorrect shift values of these areas are eliminated and interpolated from neighboring estimates, the interferometric phase quality is greatly improved (Figure 2c).

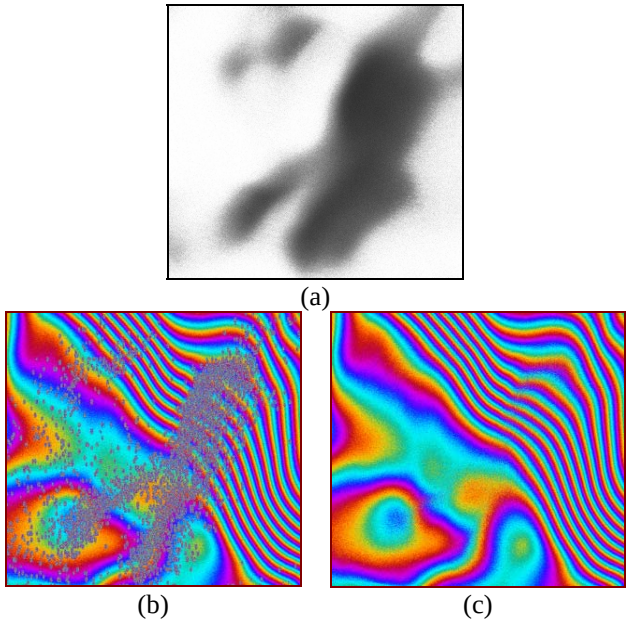

Figure 2. Detail of the processed TerraSAR-X scene at the source of RAMP glacier: (a) backscattering; (b) interferometric phase if the outliers of the resampling matrices are not eliminated; (c) interferometric phase after the outliers of the resampling matrices are removed.

3.2 Differential interferogram generation. Double difference interferometry

For the study area three consecutive repeat pass TerraSAR-X acquisitions are available on 03.12.2008, 14.12.2008 and 25.12.2008 from which two independent interferograms can be generated. The baselines and height of ambiguity are:

Interferogram 1 (3.12/14.12) B_1= - 94.5 m; h_{amb1}= - 80.1 m

Interferogram 2 (14.12/25.12) B_2= 23.5 m; h_{amb2}= 630 m

Having the same repeat interval of 11 days and different baselines, the phase due to motion can be canceled [3].

Assuming that there is no baseline error and no atmospheric distortions, the interferometric phase of both interferograms can be written as:

$$\phi_1 = \frac{4\pi}{\lambda}\frac{h \cdot B_1}{r_0 \sin\theta} + \frac{4\pi}{\lambda} d_{12},$$

$$\phi_2 = \frac{4\pi}{\lambda}\frac{h \cdot B_2}{r_0 \sin\theta} + \frac{4\pi}{\lambda} d_{23},$$

where B_1 and B_2 are the normal baselines for the interferogram 1 and 2, respectively, d_{12} is the deformation between the 1st and the 2nd acquisition, d_{23} the deformation between the 2nd and the 3rd acquisition, h corresponds to the terrain height, λ is the radar wavelength, r_0 is the range distance and θ the incidence angle.

If uniform movement and constant time intervals are assumed ($d_{12} = d_{23}$), the difference between both interferometric phases is only due to the topography:

$$\phi_{topo} = \phi_1 - \phi_2 = \frac{4\pi}{\lambda} \frac{h}{r_0 \sin\theta} B_{eq}$$

ϕ_{topo} corresponds to the topography for an interferogram with a baseline $B_{eq} = B_1 - B_2$. In order to obtain the topographical phase for the real baselines, ϕ_{topo} has to be unwrapped (ϕ_{topo}^{unw}) and scaled with the real baselines:

$$\phi_{topo1} = \phi_{topo}^{unw} \cdot \frac{B_1}{B_{eq}}, \qquad \phi_{topo2} = \phi_{topo}^{unw} \cdot \frac{B_2}{B_{eq}}. \tag{1}$$

Thus the phase corresponding to the displacement can be obtained for both interferograms as:

$$\phi_{disp}^1 = \phi_1 - \phi_{topo1} \qquad \phi_{disp}^2 = \phi_2 - \phi_{topo2}$$

Figure 3a and Figure 3b show the backscattering and the interferometric phase, respectively, while Figure 4 shows the phase separation in two components, movement (Figure 4a) and topography (Figure 4b), once it has been scaled to the baseline of the first interferogram according to Eq. 1.

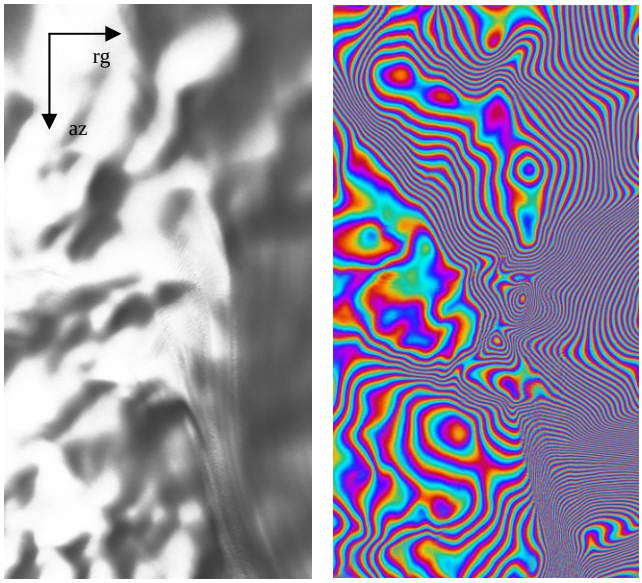

(a) (b)

Figure 3. The source of RAMP glacier corresponding to the red box in Figure 1: (a) backscattering from 03.12.2008; (b) interferometric phase based on 03.12.08 / 14.12.08 data pair. A multilooking factor of 25 was applied.

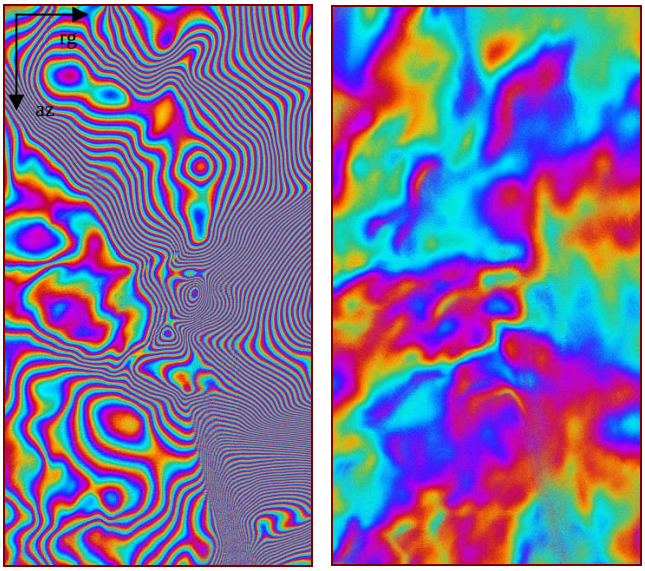

(a) (b)

Figure 4. (a) Phase due to the movement; (b) phase due to the topography based on 03.12.08/14.12.08 data pair. The height conversion factor is h_{amb}= - 80.1 m.

3.3 Determination of the absolute phase offset

After unwrapping the phase due to displacement, a reference point for the phase is necessary in order to obtain the displacement of the whole scene. In our scene, where both the ice sheet and ice stream are moving [2], no ground control point is available and a speckle tracking approach has been applied.

Speckle tracking gives a measure of the shift for every pixel due to two contributions: displacement and parallax effect. Because in our scene the terrain can be considered almost flat (Figure 4b) the shift due to the parallax effect can be modeled as a plane, defined by imaging geometry parameters, and then subtracted from the total shift. The mean height of the area from the ICESat based DEM [6] of 2000 m a.s.l. is added to the earth ellipsoid and used to generate this plane.

The deformation in range direction obtained after removing the parallax effect is shown in Figure 6. The black areas correspond to outliers due to the weak backscattering as observed in the amplitude image (Figure 3a).

The speckle tracking estimates corresponding to the displacement can be used to reference the unwrapped phase. The histogram of the difference between speckle and phase estimates is shown in Figure 5. The outliers on the left and on the right of the histogram originate from the speckle tracking estimates for the areas with low backscattering (Section 3.1). If these outliers are removed, an offset of about 638 radians is found. After subtracting this offset from the interferometric phase estimates, removing outliers and transforming to units of cm/day the

histogram of Figure 7 is obtained. A Gaussian function has been fitted to the histogram which has a standard deviation of 2.28 cm/day giving us a hint of the phase offset estimation accuracy. The standard deviation value depends mainly on the speckle tracking accuracy, which is one order of magnitude worse than the interferometric phase accuracy.

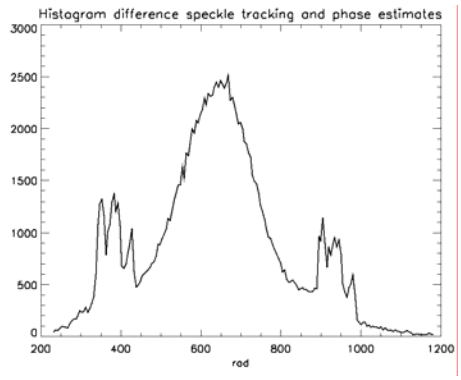

Figure 5. Histogram of the difference between speckle tracking estimates and estimates from the interferometric phase in radians.

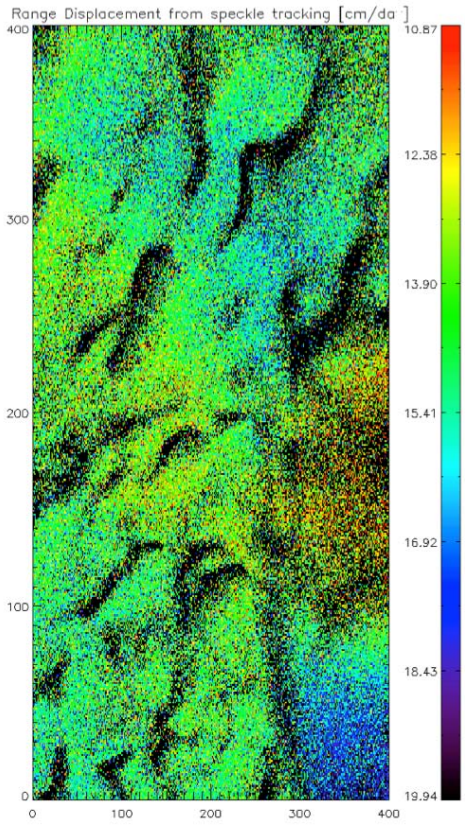

Figure 6. Range displacement from the speckle tracking technique. The black areas correspond to low backscattering, where estimation is completely erroneous.

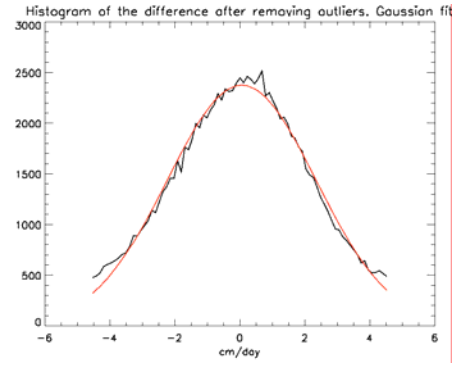

Figure 7. Histogram of the difference in cm/day between speckle tracking estimates and estimates from the interferometric phase once the offset is corrected, not taking into account the outliers. The red curve corresponds to the Gaussian fit, having a standard deviation of 2.28 cm/day.

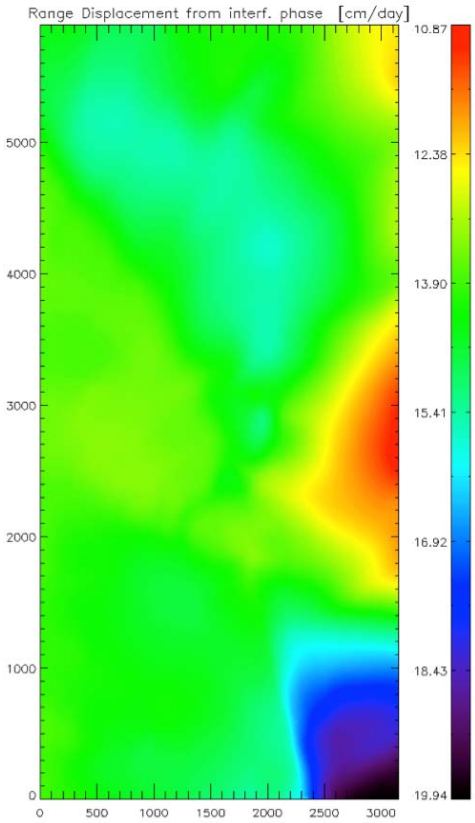

Figure 8. Range displacement from the unwrapped interferometric phase.

Figure 8 shows the displacement coming from the interferometric phase in units of cm/day. A good qualitative agreement with the displacement pattern in Figure 6 can be observed. Since both velocity maps were obtained using independent procedures, this confirms the assumption of uniform movement (section 3.2). Figure 7 shows a quantitative intercomparison between the measures coming from the speckle tracking and from the interferometric phase.

3.4 Interferometry and speckle tracking accuracy comparison

Speckle tracking and interferometric phase technique accuracies can also be compared using theory. In [4] the accuracy using coherent cross-correlation is deduced. To approximate the accuracy of the speckle tracking (incoherent cross-correlation) from the coherent cross-correlation, the Cramer-Rao bound has to be multiplied by $\sqrt{2}$. This approximation is only true for high SNR, which is not the case for our data (Figure 3a) and thus it gives only the lower limit of the accuracy in meters as:

$$\sigma_{disp\_ST} = \sqrt{\frac{3}{2 \cdot N_{patch}}} \frac{\sqrt{1-|\gamma|^2}}{\pi \cdot |\gamma|} \cdot osf^{\frac{3}{2}} \sqrt{2} \cdot \frac{c}{2 \cdot rsf} [m] \qquad (2)$$

where N_{patch} is the number of pixels of the correlation patch, λ the wavelength, γ the correlation coefficient, *osf* the oversampling factor, *c* the speed of light and *rsf* the range sampling frequency.

On the other hand, the achievable accuracy with the interferometric phase is given by [5] and expressed in meters:

$$\sigma_{disp\_\varphi} = \frac{1}{\sqrt{2 \cdot N_{ml}}} \cdot \frac{\sqrt{1-|\gamma|^2}}{|\gamma|} \cdot \frac{\lambda}{4\pi} [m] \qquad (3)$$

where N_{ml} is the multilooking factor, γ the coherence and λ the wavelength.

Figure 9 shows a comparison of the achievable accuracies given by equations 2 and 3. Interferometric phase is about 50 times more accurate than speckle tracking for the used parameters:

N_{patch}	1024
Osf	1.1
Rsf	100 MHz
N_{ml}	25
λ	3.1 cm

For a mean coherence of 0.6 the theoretical lower bound of the speckle tracking accuracy according to Eq. 2 is about 0.35 cm/day, which is much lower than the accuracy of 2.28 cm/day obtained for the real data (Figure 7). This large discrepancy is still under investigation.

4. CONCLUSION

Using the unique capabilities of TerraSAR-X, a new velocity map of a major glacier in East Antarctica has been produced. The map extends earlier studies begun in 1997 as part of the Radarsat-1 Antarctic Mapping Project. The new map reveals details of ice flow in the uppermost reaches of this unusual tributary of Recovery Glacier. After applying a double differencing approach to remove topography, a combination of speckle tracking and phase interferometry were used to obtain highly accurate estimates of velocity near the onset of fast glacier flow. Direct comparison of phase and speckle displacement data and theoretical estimates of displacement accuracy for each technique show that speckle derived velocities are accurate to a few centimeters per day.

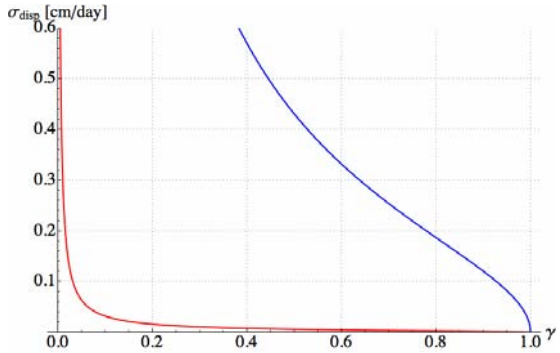

Figure 9. Comparison of lower bound of speckle tracking accuracy (Eq. 2) and interferometric phase accuracy (Eq. 3) as function of coherence.

5. REFERENCES

1. Floricioiu, D. and Jezek, K. (2009). Antarctica during the IPY: TerraSAR-X images of the Recovery Glacier system. *Environmental Geology* , 58 (2) , pp. 457-458.
2. Jezek, K, Floricioiu, D., Farness, K. Yague-Martinez, N. and Eineder, M. (2009). TerraSAR-X observations of the Recovery Glacier system, Antarctica. *IEEE International Geoscience and Remote Sensing Symposium*, 12-17 July 2009 , Cape Town, South Africa. (in press).
3. Zhao, Z., (2001). *Surface velocities of the East Antarctic Ice Streams from RADARSAT-1 interferometric synthetic aperture radar data*. Ph.D. Thesis. The Ohio State University, 180 p.
4. Bamler, R. and Eineder, M. (2005). Accuracy of Differential Shift Estimation by Correlation and Split Bandwidth Interferometry for Wideband and Delta-k SAR Systems., *IEEE Geoscience and Remote Sensing Letters*, vol. 2(2), pp. 151-155.
5. Rosen, P. et al (2000). Synthetic Aperture Radar Interferometry, *Proceedings of the IEEE*, vol. 88 (3), pp. 333-382.
6. Bamber, J.L., Gomez-Dans, J.L. and Griggs, J.A. (2008). A new 1 km digital elevation model of the Antarctic derived from combined satellite and laser data – Part 1: data and methods, *The Cryosphere Discuss.*, 2, pp 811-841.